Improved Particle Swarm Optimization Algorithm for Multi-Objective Drone Path Planning

Aihua ZHANG

College of Aeronautics and Astronautics, Geely University of China, Section 2, Chengjian Avenue, Eastern New District, Chengdu, 641423, China
zhangaihua@guc.edu.cn

Abstract: This study presents a multi-objective optimization model for drone path planning that simultaneously considers path length, flight safety, and path diversity. The drone flight environment is first modeled, followed by the construction of an optimization model based on the path length and the drone flight-related threat level. An improved Particle Swarm Optimization (PSO) algorithm is then proposed, incorporating a Sugeno function for dynamically adjusting nonlinear inertia weights and learning factors, thereby enhancing the proposed model's global search capability and drone path planning accuracy. The experimental results for two test scenarios (Maps A and B) demonstrate that the proposed algorithm identifies the optimal drone flight paths after 68 and 75 iterations, respectively, with average path lengths of 1.52 km and 1.65 km. These findings show that the enhanced PSO algorithm provides an effective and reliable solution for drone path planning, with broader implications for algorithmic optimization in related fields.

Keywords: Drone path planning, Sugeno function, Multi-objective optimization, Particle swarm optimization algorithm.

1. Introduction

With the swift advancement of drone technology, its applications in various fields are becoming increasingly widespread, such as logistics distribution, environmental monitoring, search and rescue operations, military reconnaissance. As one of the key technologies to ensure the efficient and safe completion of tasks, drone path planning has attracted significant attention in both academia and industry (Alabdalbari & Abed, 2022). In complex flight environments, drone path planning not only needs to consider the optimization of path length (PL) to save energy and time but also to minimize drone flight path-related threats to ensure flight safety, making path planning a typical multi-objective optimization problem (Jones et al., 2023). Modern heuristic algorithms, for example, an optimization algorithm based on intuition and experience, start from specific domain knowledge regarding a certain problem and search for the optimal solution through iterative exploration. This type of algorithm demonstrates significant advantages in solving complex multi-objective optimization problems, making it especially suitable for scenarios such as unmanned aerial vehicle path planning that involve multiple conflicting objectives (e.g. path length, flight time, energy consumption, and safety). The Particle swarm optimization (PSO) algorithm has significant advantages in drone path planning applications, with strong global optimization capabilities, a fast convergence, and an easy implementation of multi-objective optimization (Abu et al., 2022). It can provide safe, energy-saving, and efficient flight path solutions for drones, ensuring an efficient and safe task execution in complex environments (Liu et al., 2022). However, the existing PSO algorithms face limitations in solving multi-objective optimization problems, such as a tendency to become trapped in local optima and sensitivity to parameter settings, which poses challenges in fulfilling the stringent requirements for path planning accuracy and drone reliability in complex environments (Almazrouei et al., 2023). Therefore, in response to the shortcomings of traditional PSO algorithms, the Sugeno function is introduced to dynamically adjust inertia weights and learning factors, and combined with a reverse learning elimination mechanism, an improved PSO algorithm for multi-objective drone path planning is proposed. This study proposes an effective and reliable optimization algorithm for drone path planning in complex environments, improving the efficiency and safety of drone task execution. The novel aspect of this research consists in proposing a drone path planning model that combines multi-objective optimization related to aspects like path length, flight safety, and path diversity, and designing an improved PSO algorithm with a significantly enhanced global search capability and reaching solution optimality.

The remainder of this study is structured as follows. Section 2 systematically reviews the current research on unmanned aerial vehicle path planning and points out the limitations of different methods, providing a theoretical basis for future improvements. Section 3 mainly focuses

https://doi.org/10.24846/v35i1y202608

on the multi-objective unmanned aerial vehicle path planning optimization design based on the improved PSO algorithm. The Sugeno function is employed to dynamically adjust the inertia weights and learning factor and is combined with a reverse learning elimination mechanism to improve the global search capability and convergence accuracy. By simultaneously taking path length and drone flight-related threat level as a dual objective, a Pareto optimal model with turning angle and maximum/minimum path length constraints is established and solved using an improved PSO algorithm. Section 4 tests and analyzes the convergence speed, search accuracy, and drone path planning optimization effect of the proposed method. Finally, Section 5 analyzes and discusses the test results, and provides possible future research directions.

2. Related Works

The application of drones on modern battlefields and in civilian contexts is becoming increasingly widespread, and their path planning problem has become a research hotspot. Drone path planning is the process of planning an optimal or approximately optimal path for a drone from an initial position to a desired destination in a specific environment, in order to fulfil mission needs and accommodate environmental limitations. Due to the complexity and variability of the actual environment, as well as the presence of various threats and uncertainties, multi-objective path planning has become a key challenge in unmanned aerial vehicle mission planning. Therefore, many experts and scholars have conducted relevant research on general unmanned aerial vehicle path planning. Ait Saadi et al. (2022) conducted a review on the path planning problem of unmanned aerial vehicles, dividing the existing path planning methods into four categories: classical methods, heuristic methods, machine learning methods, and hybrid algorithms. Through the critical analysis of the objectives, constraints, and applicable environments targeted by various methods, it was found that heuristic algorithms had significant advantages in solving unmanned aerial vehicle path planning problems. Puente-Castro et al. (2022) conducted a literature review on path planning for drone swarms. By summarizing the latest and relevant research results and conducting a quantitative analysis, this study revealed the application trend of Artificial Intelligence (AI) algorithm in the area of drone cluster path planning. The results indicated that the number of research papers in this field increased in recent years, and the once most widely-used technologies no longer hold a dominant position. The AI technologies involved are mainly divided into four categories: reinforcement learning, evolutionary computing, swarm intelligence, and graph neural networks. Jiang et al. (2024) addressed the challenges faced in the field of drone path planning and proposed and analyzed relevant research on applying evolutionary computation for drone path planning in complex environments. They classified and systematically investigated specific algorithm applications in different scenarios. The results revealed the current research progress and pointed out potential research directions for applying evolutionary computing methods in this field in the future. Hu & Huang (2024) proposed an improved actor-critic reinforcement learning method to address decision-making challenges in autonomous driving scenarios. This approach can accommodate significant variations in the diverse parameters of dynamic traffic environments. The findings demonstrated that the proposed method is capable of making agile decisions that strike a balance between driving safety, efficiency, and operational constraints within complex urban settings.

The PSO algorithm, as an emerging swarm intelligence optimization algorithm, has shown considerable promise in the area of path planning due to its unique optimization mechanism and excellent global search ability. Hu et al. (2025) proposed a novel hybrid PSO for unmanned aerial vehicle path optimization. This algorithm mainly improves global optimization performance by integrating the simulated annealing algorithm. The outcomes showed that compared with other path planning algorithms, this approach could quickly plan higher quality paths for drones. Xu et al. (2022) proposed a novel method for smooth path planning for mobile robots, which combines a novel fourth-order Bezier transition curve and an improved PSO algorithm. This method uses adaptive weighted delay velocity to improve the PSO algorithm. The outcomes indicated that the research method could effectively smooth the path of mobile robots. Vijayammal et al. (2024) proposed a combined improved nonlinear dynamic inertia weight (NDIW)-based PSO algorithm for the safe path planning of unmanned aerial vehicles facing multiple threats in a 3D environment. This algorithm considers terrain and drone performance

constraints by introducing a cost function, and utilizes improved NDIWs to enhance convergence speed and fitness function values. The results showed that in complex environments, the improved NDIW PSO algorithm significantly improved convergence speed and reduced fitness function and initialization time values, and it obtained a smoother path that approaches the optimal solution.

The above research indicates that the PSO algorithm has yielded notable outcomes in drone path planning problems, yet there are still some challenges and unresolved issues. However, the standard PSO algorithm, when solving the three-dimensional multi-objective path planning for unmanned aerial vehicles, is prone to getting stuck in the local Pareto front in the search space featuring a complex terrain, dynamic threats, and multiple performance indicators due to only maintaining a single global optimal solution and lacking an effective diversity preservation mechanism. At the same time, its learning factors, inertia weights, and other parameters are highly sensitive to problem characteristics, and small disturbances can cause distortion or convergence stagnation in the solution set distribution, making it difficult to simultaneously meet the strict equilibrium requirements with regard to multiple objectives such as flight duration, energy consumption, radar exposure, and safety margin. An improved PSO algorithm is proposed for multi-objective unmanned aerial vehicle path planning, hoping to quickly obtain the optimal path for unmanned aerial vehicle flight and provide scientific and reasonable flight planning solutions for unmanned aerial vehicles.

3. Optimization Design for Multi-objective Drone Path Planning Based on Improved PSO Algorithm

3.1 Modeling of Drone Flight Environment

Modeling the drone flight environment is the foundation of path planning, especially in complex environments. Accurate environment modeling is crucial for drones to safely and efficiently perform tasks. Drone path planning in challenging environments has been widely studied (Li et al., 2023; Sudra et al., 2023), and this study focuses on this problem. By analyzing various factors that affect drone flight, a flight environment modeling method based on Digital Elevation Model (DEM) is proposed (Fang et al., 2023; Wang et al., 2024). The distinct typical procedure of this modelling method is presented in Figure 1 (Lee & Kim, 2022; Mutaqin et al., 2023).

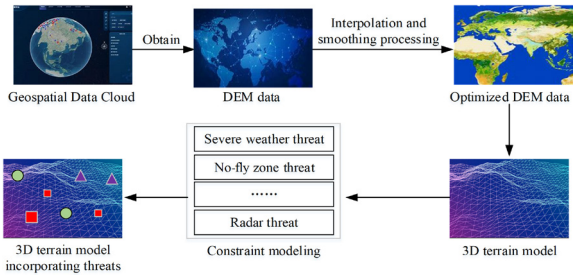

Figure 1. DEM-Based Flight Environment Modeling Process

As shown in Figure 1, DEM data is first obtained from public data sources such as geospatial data clouds, and then interpolated and smoothed to eliminate noise and discontinuity in the data, ensuring the accuracy of the terrain model. The optimized DEM data is converted into a 3D terrain model, including elevation and geographic coordinate information regarding the terrain, which is also expressed in equation (1) (Zhao et al., 2022):

$$A(x,y)=h_0+\sum_{i=1}^{N}h_i*\exp\left\{-\left[\frac{(x-x_i)}{x_{si}}\right]^2-\left[\frac{(y-y_i)}{y_{si}}\right]^2\right\} \quad (1)$$

In equation (1), $A(x,y)$ is the elevation value corresponding to the position coordinates in the 3D terrain model. h_0 is the lowest point of terrain elevation, and h_i represents the altitude of the i-th mountain peak. *exp* represents an exponential function used for calculating the impact of mountain peaks on the surrounding terrain. (x_i,y_i) represent the position coordinates of the i-th mountain in the 3D terrain model. N is the number of mountain peaks in the 3D terrain model. (x_{si},y_{si}) is the attenuation factor of the i-th peak in both the x axis and y axis directions. When flying in this 3D terrain model, drones are not only constrained by terrain obstacles, but also threatened by severe weather, no-fly zones, radar detection, and the risk of artillery bombardment. In this study the equivalent cylinder method is employed for representing the areas threatened by severe weather and the existence of no-fly zones, as expressed in equation (2) (Li et al., 2022).

$$F_m(x,y)=\begin{cases}H_{wi} & (x-x_i)^2+(y-y_i)^2>R_i\\ 0 & (x-x_i)^2+(y-y_i)^2\le R_i\end{cases} \quad (2)$$

In equation (2), $F_m(x,y)$ is the equivalent elevation value for severe weather threats and no-fly threat areas. H_{wi} is the altitude of the i-th severe weather and no-fly threat area. (x_i,y_i) represent the position coordinates of the i severe weather and no-fly threat area. R_i is the radius of the i-th severe weather and no-fly threat area. The hemispherical equivalent method is used for representing the radar detection threat area, as expressed in equation (3).

$$\begin{cases} F_r(x,y)=\sqrt{R_{\max}^2-(x-x_{r0})^2-(y-y_{r0})^2}+z_{r0} \\ R_{\max}=\left[\dfrac{P_t G^2\lambda^2\partial}{(4\pi)^3 S_{\min}}\right]^{\frac{1}{4}} \end{cases} \tag{3}$$

In equation (3), P_t represents the radar transmission power. $F_r(x,y)$ is the equivalent elevation value for the radar threat area and λ is the wavelength of electromagnetic waves. $R_{\max}$ is the radius of the radar threat area, while ∂ is the target scattering cross-sectional area. $S_{\min}$ is the minimum detectable power. (x_{r0},y_{r0},z_{r0}) represent the spatial coordinates of the radar threat area. G is the antenna gain. The threat area of shell bombardment can be represented as a spherical model, as expressed in equation (4).

$$\begin{cases} Z_{md}=R_{\max}^2-(x-x_{m0})^2-(y-y_{m0})^2 \\ Z_{md}=\begin{cases} h_{\max} & Z_{md}\geq h_{\max} \\ \sqrt{R_{\max}^2-(x-x_{m0})^2-(y-y_{m0})^2}+z_{m0} & 0\leq Z_{md}\leq h_{\max} \\ 0 & Z_{md}\leq 0 \end{cases} \end{cases} \tag{4}$$

In equation (4), Z_{md} is the equivalent elevation value of the area threatened by shell bombardment. $R_{\max}$ is the maximum threat radius. (x_{m0},y_{m0},z_{m0}) denote the center position of the projectile launch area and $h_{\max}$ is the high boundary of the artillery firing zone. The model defined in equation (4) is used to describe the drone flight space, as shown in Figure 2.

The above digital elevation map generation method can be used to obtain a 3D terrain model of the drone flight space as shown in Figure 2(a). Adding threat areas will result in a 3D terrain simulation flight environment for the drone as shown in Figure 2(b).

3.2 Improvement Analysis for the PSO Algorithm

The PSO algorithm, as a swarm intelligence-based optimization algorithm, has the advantages of easy implementation and fast convergence, and finds broad applicability in the domain of unmanned aerial vehicle path planning (Jiang et al., 2023). However, traditional PSO algorithms face problems such as being prone to local optima and being sensitive to parameter settings. Therefore, improvements are needed to meet the requirements of multi-objective drone path planning (Han & Song, 2024). To deal with the problem that traditional PSO algorithms are prone to getting stuck in local optima regions, the Sugeno function is used for adjusting the inertia weights of traditional PSO algorithms, as formulated in equation (5) (Wang et al., 2022):

$$\lambda(t)=\lambda_{\min}+(\lambda_{\max}-\lambda_{\min})\frac{1-\dfrac{t}{t_{\max}}}{1+\varepsilon*\dfrac{t}{t_{\max}}} \tag{5}$$

In equation (5), $\lambda(t)$ is a nonlinear dynamic inertia weight. In the PSO algorithm, $\lambda(t)$ controls the degree to which particles maintain their previous velocity. It directly affects the exploration and development ability of particles. $\lambda_{\max}$ and $\lambda_{\min}$ denote the maximum and minimum values of the nonlinear inertia weight, respectively. ε is a constant, while t and $t_{\max}$ represent the current iteration count and the maximum iteration count, respectively.

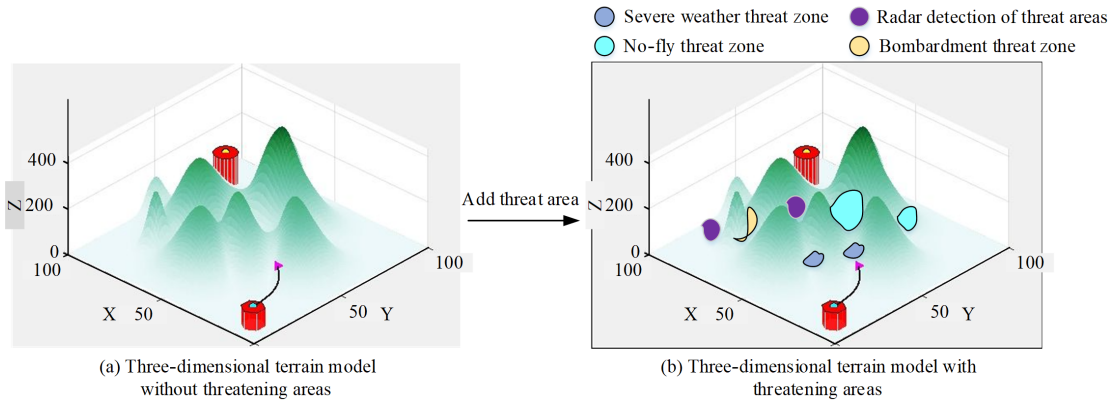

(a) Three-dimensional terrain model without threatening areas

(b) Three-dimensional terrain model with threatening areas

Figure 2. Schematic Diagram of Drone Flight Space Modeling

In response to the problem of group convergence speed for traditional PSO algorithms, this study introduces the Sugeno function to update the two learning factors in the original algorithm, as shown in equation (6) (Zhang & Zhang, 2022):

$$\begin{cases} \eta_1(t)=\eta_1(t)_{\min}+\left(\eta_1(t)_{\max}-\eta_1(t)_{\min}\right)\dfrac{1-\dfrac{t}{t_{\max}}}{1+\varepsilon*\dfrac{t}{t_{\max}}} \\ \eta_2(t)=\eta_2(t)_{\min}+\left(\eta_2(t)_{\max}-\eta_2(t)_{\min}\right)\dfrac{1-\dfrac{t}{t_{\max}}}{1+\varepsilon*\dfrac{t}{t_{\max}}} \end{cases} \quad (6)$$

In equation (6), $\eta_1(t)$ and $\eta_2(t)$ are learning factors. $\eta_1(t)_{\max}$ and $\eta_2(t)_{\max}$ are the maximum values of the learning factors. $\eta_1(t)_{\min}$ and $\eta_2(t)_{\min}$ are the minimum values of the learning factors. This improvement allows the algorithm to maintain a high level of exploration ability in the early stages of the search, in order to conduct precise searches in the vicinity of the global optimum. To bring the updated particles closer to the global optimal solution, this study introduces a reverse learning elimination mechanism to improve the traditional PSO algorithm. The updated number of eliminated particles is given by equation (7) (Piao, 2024):

$$k\in\left[\frac{N}{\gamma},\frac{N}{0.618\gamma}\right] \quad (7)$$

In equation (7), k represents the number of eliminated particles. N is the number of individual particles, and γ is the updated scaling factor. The improved PSO algorithm operation flow is presented in Figure 3.

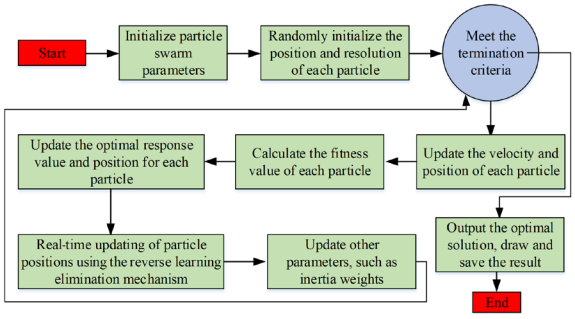

Figure 3. Improved PSO Algorithm Operation Flow

As shown in Figure 3, the improved PSO algorithm first initializes a population containing n particles and sets their positions and velocities. Next, the fitness value of each particle is calculated and the individual optimal position and global optimal position are updated. Then, the inertia weight and learning factor of the particles are adjusted according to equations (5) and (6), the velocity and position of the particles are calculated and updated, and the particle position is optimized using the reverse learning elimination mechanism in equation (7). Finally, the termination criteria are checked to see if they are met by the algorithm. If they are met, the algorithm execution is stopped. Otherwise, the above steps are repeated.

3.3 Construction of a Multi-objective Optimization Model for Drone Path Planning Based on an Improved PSO Algorithm

The above method was already applied for the 3D modeling of the flight environment of drones, and drone path optimization usually involves two conflicting evaluation indicators: the path length and path-related threats (Luo et al., 2024; Zhang, 2024). To this end, this study constructed an optimization model based on the dual criteria of path length and path-related threats, and then it employed the improved PSO algorithm to solve the optimization model and find a set of Pareto optimal paths (Shao et al., 2022). The path of the drone can be viewed as a continuous 3D coordinate system and digitized using real number encoding, as shown in Figure 4 (Hu & Minner, 2023).

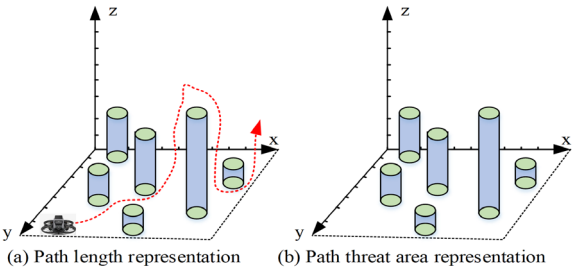

(a) Path length representation (b) Path threat area representation

Figure 4. Drone Path Length and Path Threat Area Representation Method for Unmanned Aerial Vehicles

As shown in Figure 4(a), the red dashed line represents the total length of the drone's flight path, which can be represented by continuous 3D coordinates (x_0,y_0,z_0), (x_1,y_1,z_1), (x_2,y_2,z_2)... (x_n,y_n,z_n). When optimizing drone path planning, it is necessary to ensure the shortest path length to save fuel consumption and time, so the cost of setting the path length is given by equation (8) (Bi et al., 2023):

$$P_L=\sum_{a=1}^{N\text{var}-1}\sqrt{\left[x_{a+1}-x_a\right]^2+\left[y_{a+1}-y_a\right]^2+\left[z_{a+1}-z_a\right]^2} \quad (8)$$

In equation (8), P_L represents the cost of setting the drone path length. Nvar is the number of drone path waypoints. Nvar−1 is the number of path segments on a path. The cylinders in Figure 4(b) represent the threat areas, which can also be represented by continuous 3D coordinates. The cost of setting the threat area is given by equation (9) (Chai & Xia, 2023):

$$f_T = \sum_{a=1}^{N\text{var}} \sum_{b=1}^{Num} \frac{10 r_b}{dis_{ab}}, \tag{9}$$

In equation (9), f_T is the cost of setting the drone threat area. Nvar is the number of drone path waypoints. Num represents the number of threat areas. r_b is the radius of the b-th threat area. dis_{ab} is the distance between the a-th path point on the drone's path and the b-th threat area. Grounded on the above analysis, a drone path optimization model is constructed as shown in equation (10) (Shen et al., 2024):

$$E_{\min} = P_L + f_T \tag{10}$$

In equation (10), $E_{\min}$ is the objective function for optimization. To this end, constraints need to be added to the drone path optimization model, as shown in Figure 5 (Aljalaud et al., 2023; Shang & Shen, 2023):

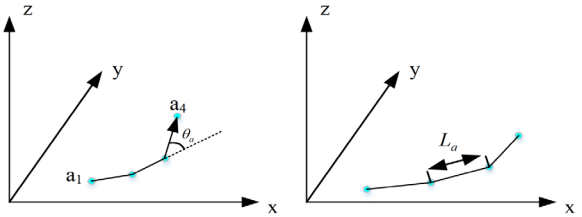

Figure 5. Schematic Diagram of Constraint Conditions for the Unmanned Aerial Vehicle Path Optimization Model

Figure 5(a) shows the maximum turning angle constraint during flight, as expressed in equation (11) (Lin et al., 2024):

$$\theta_{\min} \le \theta_a \le \theta_{\max} \tag{11}$$

In equation (11), θ_a is the size of the turning angle at the a-th path point on the drone's path.

The maximum path length constraint during drone flight is shown in Figure 5(b) and expressed in equation (12) (Zhou et al., 2022):

$$\sum_{a=1}^{N\text{var}-1} L_a \le L_{\max} \tag{12}$$

In equation (12), L_a is the length of the a-th flight path, which is the straight-line distance from the a-th path point to the a+1-th path point. $L_{\max}$ is the maximum allowable path length for drone flight, which ensures that the drone can safely complete its flight. The minimum path length constraint during flight is given by equation (13) (Luo et al., 2023):

$$L_a \ge L_{\min} \tag{13}$$

In equation (13), $L_{\min}$ is the minimum allowable path length for drone flight. After constructing the drone path optimization model, each particle influenced by the improved PSO algorithm is regarded as a planned flight path with countless scattered points, and the x, y, and z coordinates of the path points are randomly generated (Wang et al., 2022). Afterwards, the improved PSO algorithm is updated and iterated, and the optimal flight path that fulfills the criteria of the objective function is finally generated.

In the initialization stage, the population size N is set at 100, and each particle is composed of 20 three-dimensional trajectory nodes (x, y, z) encoded with real numbers. The maximum number of iterations is Tmax=100. The inertia weight decreases nonlinearly between [0.9, 0.4] according to equation (5), and the learning factors η_1 and η_2 are dynamically adjusted between [0.9, 2.5], respectively. In the reverse learning elimination mechanism, the scaling factor γ is set at 0.6, and the proportion of eliminated particles does not exceed 15% of the current population. The termination criterion is triggered by a dual condition of "maximum number of iterations or no significant improvement in 50 consecutive Pareto frontiers". Ultimately, the optimal flight path that satisfies the objective function criteria is obtained.

4. Improved PSO Algorithm Performance and Application Analysis

4.1 Analysis of Convergence Speed and Search Accuracy Results for the Improved PSO Algorithm

To confirm the validity of the improved PSO algorithm, the most representative single-mode benchmark test function $F_1 = \sum_{i=1}^{n} x_i^2$ and the multi-modal benchmark test function $F_2 = \sum_{i=1}^{n} -x_i \sin\left(\sqrt{|x_i|}\right)$ were selected as the test

functions for algorithm performance. The test environment and parameter settings are presented in Table 1.

Table 1. Working Conditions of the proposed Model

Project	Parameter
System	Windows 8
GPU	RTX 4090
CPU	i9-13900K
Memory	DDR5 6400 32GB(16GBx2
Motherboard	ROG MAXIMUS Z790 HERO

In the operating environment of Table 1, the traditional PSO algorithm, the improved Inertia Weight PSO algorithm (IIWPSO), the improved Learning Factor PSO algorithm (ILFPSO), the Improved PSO algorithm in this study (IPSOIS), the improved GWO algorithm (IGWO), and the improved NSGA-II algorithm (INSGA-II) were run 100 times on the benchmark test functions F_1 and F_2. The outcomes are included in Table 2.

As presented in Table 2, Best refers to the optimal solution (minimum value) found by the algorithm in 100 independent runs. This value represents the best performance that the algorithm can achieve over multiple attempts. Worst refers to the worst solution (maximum value) found by the algorithm in 100 independent runs. This value reflects the worst performance achieved by the algorithm. Average value refers to the arithmetic mean of the solutions found by the algorithm over 100 independent runs. This indicator comprehensively reflects the overall average performance of the algorithm. Standard deviation refers to the standard deviation of the solution found by the algorithm in 100 independent runs. This indicator measures the degree of dispersion or the stability of the algorithm results.

For the two test functions above, the Best values of IPSOIS were 2.82E-02 and 9.96E-01, respectively. These values reflect a higher accuracy in comparison with the Best values of other algorithms such as PSO, IIWPSO, ILFPSO, IGWO, and INSGA-II. For the test function F_1, the standard deviation of IPSOIS is only 1.32E-01, the standard deviation of IPSOIS (1.32E-01) is significantly lower than that of PSO (2.63E+24) and IIWPSO (2.14E+22), indicating an improved stability of the algorithm. And although ILFPSO achieves a lower Best value (3.24E-23), its Worst value reaches 4.10E+23, revealing a high fluctuation and instability. In contrast, the range of the results obtained by IPSOIS is between 2.82E-02 and 1.32E-01, and the stability improvement is significant. For the test function F_2, the standard deviation of IPSOIS (2.24E+01) is lower than that of PSO (2.71E+01) and significantly lower than that of INSGA-II (3.82E+03), further demonstrating the effectiveness of IPSOIS in handling complex multimodal optimization

Table 2. Outcomes for Different Algorithms Running on Benchmark Test Functions

F_1				
Algorithm type	Best	Worst	Average Value	Standard Deviation
PSO	4.63E-02	3.26E+22	1.36E-13	2.63E+24
IIWPSO	3.62E-13	4.26E+19	2.63E+22	2.14E+22
ILFPSO	3.24E-23	4.10E+23	3.55E-19	2.19E-18
IPSOIS	2.82E-02	8.63E-06	7.68E+03	1.32E-01
IGWO	2.96E-11	7.92E-12	5.66E-12	1.45E-09
INSGA-II	3.06E-10	7.66E-11	6.14E-19	1.63E-10
F_2				
Algorithm type	Best	Worst	Average Value	Standard Deviation
PSO	9.98E-01	1.17E+01	2.18E+00	2.71E+01
IIWPSO	9.96E-01	1.07E+01	2.18E+00	2.82E+00
ILFPSO	9.88E-01	1.27E+01	1.12E+01	3.82E+00
IPSOIS	9.96E-01	1.17E+01	4.19E+00	2.24E+01
IGWO	9.97E-01	1.07E+01	1.42E+01	2.89E+00
INSGA-II	9.98E-01	1.01E+01	2.12E+01	3.82E+03

problems. The convergence curves of IPSOIS and three other algorithms for the two benchmark test functions are shown in Figure 6.

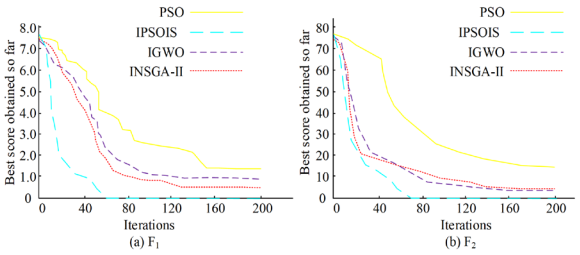

Figure 6. Convergence Curves of Different Algorithms for the Benchmark Test Functions

Regarding the performance comparison for the single-mode benchmark test function F_1 shown in Figure 6(a), IPSOIS successfully converged to the global optimal solution after only about 68 iterations. In contrast, PSO, IGWO, and INSGA-II required up to 173, 131, and 128 iterations, respectively, to achieve the same optimal solution. This indicates that the IPSOIS was significantly faster than the other three algorithms in finding the global optimal solution when dealing with such unimodal optimization problems. Further on, the analysis for the multi-modal benchmark test function F_2 depicted in Figure 6(b) shows that the IPSOIS algorithm also performed well, reaching the global optimal solution after approximately 75 iterations. This performance was better than that of IGWO and INSGA-II, which required 161 and 168 iterations, respectively to converge. The standard PSO algorithm failed to successfully find the global optimal solution for this test function, highlighting the superiority and robustness of IPSOIS in dealing with complex multi-modal optimization problems. This was because the IPSOIS, after the proposed improvements, featured efficient search strategies, optimized iterative mechanisms, and powerful global search capabilities. These advantages made the IPSOIS more efficient and accurate in solving complex optimization problems.

4.2 Analysis of the Optimization Effect on Drone Path Planning

To further verify the actual optimization effect of the IPSOIS algorithm proposed in this study, two commonly used simulated flight maps, A and B, were selected as test maps. Map A shows a mountainous terrain including 8 peaks and 4 threat areas. Map B shows a plateau terrain including 18 peaks and 8 threat areas. The top view of the optimal route for the drone obtained by the four algorithms also employed in subsection 4.1 is shown in Figure 7.

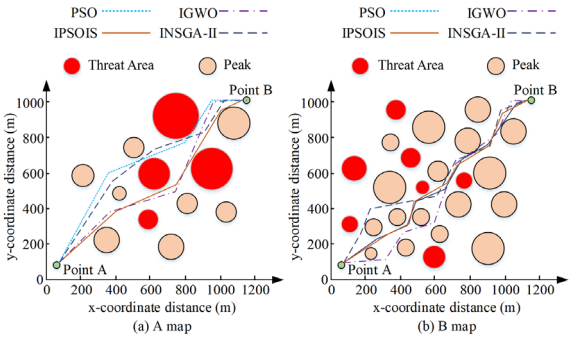

Figure 7. Top View of the Optimal Drone Route Calculated by the Four Employed Algorithms

As shown in Figure 7(a), Map A includes fewer mountain peaks and threat areas. The traditional PSO and the INSGA-II algorithm chose a relatively safe path as the optimal path, but this path was longer. IPSOIS and IGWO simultaneously considered security and path threats, selecting a relatively straight route as the optimal path. As shown in Figure 7(b), there were considerably more mountain peaks and threat areas on Map B. PSO and INSGA-II still chose the relatively safe but longer path as the optimal path, while IPSOIS selected the optimal path while ensuring safety. In the context of maps A and B, the four algorithms were run 30 times, and the optimal and average paths obtained by each algorithm are shown in Figure 8.

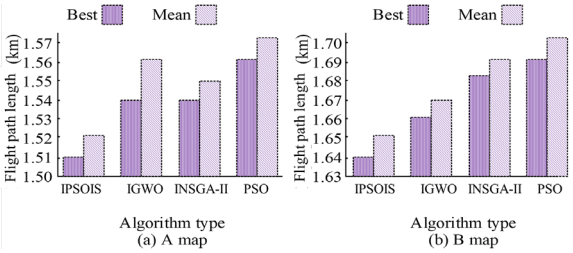

Figure 8. Comparison of Optimal Path and Average Path Length Results Calculated by the Four Algorithms

As shown in Figure 8(a), in the path optimization problem of Map A, IPSOIS, with its search strategy and high accuracy, achieved an optimal path length of only 1.51 km. In comparison with IGWO (1.54 km), INSGA-II (1.54 km), and PSO (1.56 km), the outcome was better. Meanwhile, from the perspective of the average path length, the average value obtained by IPSOIS was 1.52 km, which was also better than the average values obtained by the

other three algorithms, further demonstrating its stability and reliability. For the path optimization problem of Map B shown in Figure 8(b), IPSOIS continued to demonstrate excellent performance. Although the complexity of Map B was higher, IPSOIS still achieved an optimal path length of 1.64 km, which once again demonstrated its powerful path planning capability. In comparison with IGWO (1.66 km), INSGA-II (1.68 km), and the traditional PSO algorithm (1.69 km), IPSOIS obtained the shortest path. In addition, the average path length of IPSOIS was 1.65 km, which was also better than that of the other algorithms. This further demonstrates the wide applicability and advantages of the IPSOIS algorithm for different maps and path planning problems. The optimal and average flight times were calculated again, as shown in Figure 9.

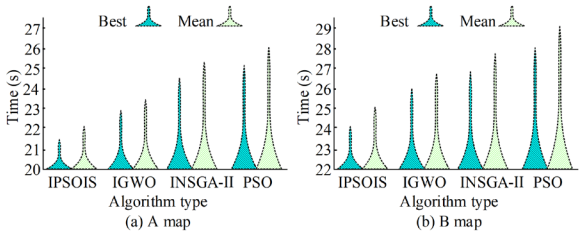

Figure 9. Comparison of the Optimal Flight Time and Average Flight Time Results Calculated by the Four Algorithms

As shown in Figure 9(a), for Map A, the optimal flight time calculated by IPSOIS was 21.5 seconds, significantly better than the values obtained by IGWO (22.9 seconds), INSGA-II (24.3 seconds), and PSO (24.9 seconds). Meanwhile, IPSOIS also achieved the shortest average path flight time, namely 22.0 seconds, showing a higher efficiency compared with IGWO (23.4 seconds), INSGA-II (25.2 seconds), and PSO (26.2 seconds). Similarly, for Map B shown in Figure 9(b), IPSOIS achieved the optimal flight time of 24.0 seconds, which was better than the values obtained by IGWO (25.9 seconds), INSGA-II (26.6 seconds), and PSO (27.7 seconds). With regard to the average path flight time, IPSOIS also obtained the shortest time, with an average of 25.0 seconds, lower than the values obtained by IGWO (26.7 seconds), INSGA-II (27.5 seconds), and PSO (29.0 seconds). This was because the IPSOIS algorithm selected straight flight paths as much as possible while ensuring safety, reducing the turning time and achieving shorter flight times. Finally, after calculating the optimal and average path length, and the optimal and average flight time, the number of nodes, and the path planning success rate were calculated by the four algorithms, the outcomes being included in Table 3.

According to Table 3, there were significant differences in the path planning performance among the four algorithms for both Map A and Map B. For Map A, IPSOIS performed the best in terms of the optimal path length, average path length, optimal flight time, and average flight time. At the same time, it obtained the lowest number of nodes and the highest path planning success rate, reaching 100%. In contrast, the PSO algorithm

Table 3. Statistical Table of Calculation Outcomes of Different Algorithms

A map				
Project	PSO	IGWO	INSGA-II	IPSOIS
Optimal Path Length	1.56 km	1.54 km	1.54 km	1.51 km
Average Path Length	1.57 km	1.56 km	1.55 km	1.52 km
Optimal Flight Time	24.9s	22.9s	24.3s	21.5s
Average Flight Time	26.2s	23.4s	25.2s	22.0s
Number of Nodes	22	14	15	9
Path Planning Success Rate	95%	99%	99%	100%
B map				
Project	PSO	IGWO	INSGA-II	IPSOIS
Optimal Path Length	1.69 km	1.66 km	1.68 km	1.64 km
Average Path Length	1.70 km	1.67 km	1.68 km	1.65 km
Optimal Flight Time	27.7s	25.9s	26.6s	24.0s
Average Flight Time	29.0s	26.7s	27.5s	25.0s
Number of Nodes	35	30	29	16
Path Planning Success Rate	92%	97%	96%	100%

performed relatively poorly on these metrics. For Map B, the IPSOIS algorithm also demonstrated excellent performance, not only maintaining a leading position with regard to the path length and flight time, but also having the lowest number of nodes and a path planning success rate of 100%. The IGWO and INSGA-II algorithms were close to IPSOIS in terms of some indicators, but overall there was still a certain gap. The performance of PSO for Map B was also inferior to that of the other three algorithms. In summary, the IPSOIS algorithm performed well for both maps and it proved to be the best algorithm for drone path planning problems.

5. Conclusion

This study proposes a solution grounded on an improved PSO algorithm for multi-objective optimization problems in drone path planning. By modeling the flight environment of unmanned aerial vehicles, a multi-objective optimization model was established with path length and drone flight-related threat level as optimization indicators, and a corresponding improved PSO algorithm was designed. This optimization algorithm utilized a Sugeno function to construct nonlinear inertia weights and learning factors, and incorporated a reverse learning elimination mechanism to improve its convergence speed and search accuracy. The test outcomes showed that for Maps A and B, the improved PSO algorithm was able to find the optimal path after 68 and 75 iterations, respectively. Also, for Maps A and B the average length of the optimal path was 1.52 km and 1.65 km, respectively. In comparison with the traditional PSO algorithm, the IIWPSO algorithm, the ILFPSO algorithm, the IGWO algorithm, and the INSGA-II algorithm, the proposed improved PSO algorithm had a better performance with regard to the convergence speed, search accuracy, flight path length, and flight time. Besides, the algorithm maintained a maximum path planning success rate of 100% on two maps of different complexities. In summary, the improved PSO algorithm proposed in the study validly addressed the challenges of path planning in complex terrain environments and provided efficient and safe flight path solutions for unmanned aerial vehicles.

Although the proposed improved PSO algorithm achieved a high success rate for static terrain, there are still two limitations. First, this study was only validated in two-dimensional static scenarios and did not consider the challenges of real-time reprogramming caused by dynamic disturbances such as sudden changes in wind speed and sudden threats. Second, the proposed algorithm still mainly relies on centralized single-run optimization, as its on-board implementation on an embedded platform under computational and communication constraints was not tested yet. Therefore, in the future, the current two-dimensional static scenario may be extended to three-dimensional dynamic scenarios, introducing disturbance models such as sudden changes in wind speed and sudden threats, and constructing a mechanism that can trigger real-time replanning. At the same time, the centralized single-run optimization framework may be integrated into the onboard embedded platform, and lightweight distributed algorithms may be designed for computing communication constraints. The real-time implementation and robustness of the algorithm can be verified through hardware-in-the-loop simulations and real drone flight experiments, thereby achieving a leap from “offline high precision” to “online strong real-time implementation.”

REFERENCES

Abu, N. S., Bukhari, W. M., Adli, M. H. et al. (2022) A comprehensive overview of classical and modern route planning algorithms for self-driving mobile robots. *Journal of Robotics and Control*. 3(5), 666–678. https://doi.org/10.18196/jrc.v3i5.14683.

Ait Saadi, A., Soukane, A., Meraihi, Y. et al. (2022). UAV PP using optimization approaches: A survey. *Archives of Computational Methods in Engineering*. 29(6), 4233–4284. https://doi.org/10.1007/s11831-022-09742-7.

Alabdalbari, A. A. & Abed, I. A. (2022) New robot path planning optimization using hybrid GWO-PSO algorithm. *Bulletin of Electrical Engineering and Informatics*. 11(3), 1289–1296. https://doi.org/10.11591/eei.v11i3.3677.

Aljalaud, F., Kurdi, H. & Youcef-Toumi, K. (2023) Bio-inspired multi-UAV path planning heuristics: A review. *Mathematics*. 11(10), 2356-2365. https://doi.org/10.3390/math11102356.

Almazrouei, K. S., Nassif, A. B. & AlShabi, M. (2023) Path-planning and obstacle avoidance algorithms for UAVs: A systematic literature review. *Unmanned Systems Technology XXV* (*Proceedings of SPIE*, vol. 12549). Bellingham, USA, SPIE, 277–284. https://doi.org/10.1117/12.2664056.

Bi, Q.L., Lai, M.L., Chen, K. et al. (2023) Spatial position recognition method of semi-transparent and flexible workpieces: A machine vision based on red light assisted. *Advances in Production Engineering & Management*. 18(1), 49-65. https://doi.org/10.14743/apem2023.1.456.

Chai, G.F. & Xia, Y.Z. (2023) Multi-Robot Path Optimization and Simulation for Multi-Route Inspection in Manufacturing. *International Journal of Simulation Modelling*. 22(1), 121-132. https://doi.org/10.2507/IJSIMM22-1-CO1.

Fang, X., Gu, Z., & Zhu, Y. (2023) Quantification of Agricultural Terrace Degradation in the Loess Plateau Using UAV-Based Digital Elevation Model and Imagery. *Sustainability*. 15(14), 10800. https://doi.org/10.3390/su151410800.

Han, Y., & Song, T. (2024) Path Planning for Shop-Floor Material Transfer Robots Incorporating Particle Swarm and Ant Colony Algorithms. *Studies in Informatics and Control*. 33(3), 49-59. https://doi.org/10.24846/v33i3y202405.

Hu, D. & Minner, J. (2023) UAVs and 3D City Modeling to Aid Urban Planning and Historic Preservation: A Systematic Review. *Remote Sensing*. 15(23), 5507-5511. https://doi.org/10.3390/rs15235507.

Hu, R., & Huang, P. (2024) Autonomous driving decision-making based on an improved actor-critic algorithm. *Studies in Informatics and Control*. 33(4), 37–50. https://doi.org/10.24846/v33i4y202404.

Hu, G., Cheng, M., Houssein, E. H., & Jia, H. (2025) CMPSO: A novel co-evolutionary multigroup particle swarm optimization for multi-mission UAVs path planning. *Advanced Engineering Informatics*. 63, 102923. https://doi.org/10.1016/j.aei.2024.102923.

Jiang, Z., Chen, Y., Wang, K. et al. (2023) A Graph-Based PPO Approach in Multi-UAV Navigation for Communication Coverage, *International Journal of Computers Communications & Control*. 18(6), 5505. https://doi.org/10.15837/ijccc.2023.6.5505.

Jiang, Y., Xu, X. X., Zheng, M. Y. et al. (2024) Evolutionary computation for unmanned aerial vehicle path planning: A survey. *Artificial Intelligence Review*, 57(10), 267–268. https://doi.org/10.1007/s10462-024-10913-0.

Jones, M., Djahel, S., & Welsh, K. (2023) Path-planning for unmanned aerial vehicles with environment complexity considerations: A survey. *ACM Computing Surveys*, 55(11), 1–39. https://doi.org/10.1145/3570723.

Lee, H. & Kim, D. (2022) Generation of Dense and High-Precision Digital Elevation Model Using Low-Cost Unmanned Aerial Vehicle and Space-Borne TanDEM-X to Measure Exposed Area Change Due to Tidal Invasion. *IEEE Journal of Selected Topics in Applied Earth Observations and Remote Sensing*, 15(1), 6899-6911. https://doi.org/10.1109/JSTARS.2022.3195744.

Li, Y., Zhang, Y., Wang, L. et al. (2022) Research on potential ground risk regions of aircraft crashes based on ADS-B flight tracking data and GIS. *Journal of Transportation Safety & Security*, 14(1), 152-176. https://doi.org/10.1080/19439962.2020.1754981.

Li, K., Li, D., & Ma, H.Q. (2023) An improved discrete particle swarm optimization approach for a multi-objective optimization model of an urban logistics distribution network considering traffic congestion. *Advances in Production Engineering & Management*, 18(2), 211-224. https://doi.org/10.14743/apem2023.2.468.

Lin, C., Jhang, J., & Chuang, C. (2024) Navigation Control of an Autonomous Ackerman Robot in Unknown Environments by Using a Lidar-Sensing-Based Fuzzy Controller. *Computer Science and Information Systems*, 21(2), 473–490. https://doi.org/10.2298/CSIS220826008L.

Liu, X., Zhang, D., Zhang, T. et al. (2022) A new path plan method based on hybrid algorithm of reinforcement learning and particle swarm optimization. *Engineering Computations*, 39(3), 993–1019. https://doi.org/10.1108/EC-09-2020-0500.

Luo, J., Wang, Z., Xia, M. et al. (2023) Path planning for UAV communication networks: Related technologies, solutions, and opportunities. *ACM Computing Surveys*, 55(9), 1-37. https://doi.org/10.1145/3560261.

Luo, J., Tian, Y., & Wang, Z. (2024) Research on Unmanned Aerial Vehicle Path Planning. *Drones*, 8(2), 51-55. https://doi.org/10.3390/drones8020051.

Mutaqin, B.W., Isnain, M.N., Marfai, M.A. et al. (2023) Assessing the accuracy of open-source digital elevation models for the geomorphological analysis of very small islands of Indonesia. Applied Geomatics, 15(4), 957-974. https://doi.org/10.1007/s12518-023-00533-8.

Piao, L. (2024) Remora Optimization Algorithm-based Adaptive Fusion via Ant Colony Optimization for Traveling Salesman Problem. *Computer Science and Information Systems*, 21(4), 1651–1672. https://doi.org/10.2298/CSIS240314052P.

Puente-Castro, A., Rivero, D., Pazos, A. et al. (2022) A review of artificial intelligence applied to path planning in UAV swarms. *Neural Computing and Applications*, 34(1), 153–170. https://doi.org/10.1007/

s00521-021-06569-4.

Shang, Z., & Shen, Z. (2023) Topology-based UAV path planning for multi-view stereo 3D reconstruction of complex structures. *Complex & Intelligent Systems*, 9(1), 909-926. https://doi.org/10.1007/s40747-022-00831-5.

Shao, Q., Li, J., Li, R. et al. (2022) Study of urban logistics drone path planning model incorporating service benefit and risk cost. *Drones*, 6(12), 418-421. https://doi.org/10.3390/drones6120418.

Shen, G.C., Liu, J., Ding, Y.L. et al. (2024) Continuous Path Planning for Multi-Robot in Intelligent Warehouse. *International Journal of Simulation Modelling*, 23(2), 323-334. https://doi.org/10.2507/IJSIMM23-2-CO6.

Sudra, P., Demarchi, L., Wierzbicki, G. et al. (2023) A Comparative Assessment of Multi-source Generation of Digital Elevation Models for Fluvial landscapes Characterization and Monitoring. *Remote Sensing*, 15(7), 1949-1955. https://doi.org/10.3390/rs15071949.

Vijayammal, B.K.P., Cherukupalli, K., Jayaraman, R. et al. (2024) A Multi-Objective Approach with Modified Particle Swarm Optimization and Hybrid Energy Systems. *Tehnicki vjesnik [Technical Gazette]*, 31(5), 1576-1581. https://doi.org/10.17559/TV-20231213001205.

Wang, J., Li, Y., Li, R. et al. (2022) Trajectory planning for UAV navigation in dynamic environments with matrix alignment Dijkstra. *Soft Computing*, 26(22), 12599-12610. https://doi.org/10.1007/s00500-022-07224-3.

Wang, Y., Li, W., & Jiang, R. (2022) A novel hybrid algorithm based on improved particle swarm optimization algorithm and genetic algorithm for multi-UAV path planning with time windows. In: *2022 IEEE 5th Advanced Information Management, Communicates, Electronic and Automation Control Conference (IMCEC)*, 16-18 December 2022, Chongqing, *China*. New York, USA, IEEE. pp. 1005-1009.

Wang, W., Zhou, C., He, H. et al. (2024) Advancing UAV Image Semantic Segmentation with an Improved Multiscale Diffusion Model. *Tehnicki vjesnik [Technical Gazette]*, 31(6), 1859-1865. https://doi.org/10.17559/TV-20231023001051.

Xu, L., Cao, M., & Song, B. (2022) A new approach to smooth path planning of mobile robot based on quartic Bezier transition curve and improved PSO algorithm. *Neurocomputing*, 473(1), 98-106. https://doi.org/10.1016/j.neucom.2021.12.016.

Zhao, X., Zhou, Q., Dong, J. et al. (2022) Digital Elevation Model-Assisted Aerial Triangulation Method On An Unmanned Aerial Vehicle Sweeping Camera System. *The Photogrammetric Record*, 37(178), 208-227. https://doi.org/10.1111/phor.12419.

Zhang, W., & Zhang, W. (2022) An efficient UAV localization technique based on particle swarm optimization. *IEEE Transactions on Vehicular Technology*, 71(9), 9544-9557. 10.1109/TVT.2022.3178228.

Zhang, H.Q. (2024) Optimizing obstacle avoidance path planning for intelligent mobile robots in multi-obstacle environments. *Advances in Production Engineering & Management*, 19(3), 358-370. https://doi.org/10.14743/apem2024.3.512.

Zhou, Q., Lo, L.Y., Jiang, B. et al. (2022) Development of fixed-wing UAV 3D coverage paths for urban air quality profiling. *Sensors*, 22(10), 3630-3635. https://doi.org/10.3390/s22103630.